ADVANCED HEALTHCARE MATERIALS
www.advhealthmat.de

Analysis of Osteoclastogenesis/Osteoblastogenesis on Nanotopographical Titania Surfaces

*Robert K. Silverwood, Paul G. Fairhurst, Terje Sjöström, Findlay Welsh, Yuxin Sun, Gang Li, Bin Yu, Peter S. Young, Bo Su, Robert M. D. Meek, Matthew J. Dalby, and Penelope M. Tsimbouri**

A focus of orthopedic research is to improve osteointegration and outcomes of joint replacement. Material surface topography has been shown to alter cell adhesion, proliferation, and growth. The use of nanotopographical features to promote cell adhesion and bone formation is hoped to improve osteointegration and clinical outcomes. Use of block-copolymer self-assembled nanopatterns allows nanopillars to form via templated anodization with control over height and order, which has been shown to be of cellular importance. This project assesses the outcome of a human bone marrow-derived co-culture of adherent osteoprogenitors and osteoclast progenitors on polished titania and titania patterned with 15 nm nanopillars, fabricated by a block-copolymer templated anodization technique. Substrate implantation in rabbit femurs is performed to confirm the in vivo bone/implant integration. Quantitative and qualitative results demonstrate increased osteogenesis on the nanopillar substrate with scanning electron microscopy, histochemical staining, and real-time quantitative reverse-transcription polymerase chain reaction analysis performed. Osteoblast/osteoclast co-culture analysis shows an increase in osteoblastogenesis-related gene expression and reduction in osteoclastogenesis. Supporting this in vitro finding, in vivo implantation of substrates in rabbit femora indicates increased implant/bone contact by ≈20%. These favorable osteogenic characteristics demonstrate the potential of 15 nm titania nanopillars fabricated by the block-copolymer templated anodization technique.

1. Introduction

It has become a prime focus of orthopedic research to improve the integration of prostheses or implants into bone and thus improve lifespans and outcomes of joint replacements. Common failure mechanisms include soft tissue production from mesenchymal stem cells (MSCs) in response to implants, resulting in soft tissue encapsulation, or osteolysis and loosening secondary to immune responses to arthroplasty wear particles.[1] Thus, further research into improving osteointegration onto implants and minimizing host immune response is vital.

Altering properties of a substrate's surface such as chemistry, stiffness, and nanoscale topography have been shown to alter cellular responses such as adhesion, proliferation, and differentiation.[2–7]

Considering metallic materials for load bearing implant application, although chemical modification of implant surface, e.g., hydroxyapatite film or coating is a widely used method, nanoscale topography as a physical

R. K. Silverwood, P. G. Fairhurst, F. Welsh, P. S. Young, Prof. M. J. Dalby, Dr. P. M. Tsimbouri
Centre for Cell Engineering
Joseph Black Building
University of Glasgow
Glasgow G12 8QQ, UK
E-mail: penelope.tsimbouri@glasgow.ac.uk

Dr. T. Sjöström
Prof. B. Su
Biomaterials Engineering Group
School of Oral and Dental Sciences
University of Bristol
Lower Maudlin Street, Bristol BS1 2LY, UK

Dr. Y. Sun, Prof. G. Li
Department of Orthopaedics and Traumatology
Li Ka Shing Institute of Health Sciences
The Chinese University of Hong Kong
Prince of Wales Hospital, Hong Kong, P. R. China

Prof. G. Li
The Chinese University of Hong Kong
Shenzhen Research Institute
Shenzhen, P. R. China

Dr. B. Yu
Department of Orthopaedic Surgery
Southern Medical University
Southern Hospital
Guangzhou, P. R. China

R. M. D. Meek
Department of Orthopaedics and Trauma
Southern General Hospital
Glasgow G51 4TF, UK

DOI: 10.1002/adhm.201500664

cue on the surface of the metallic implant is an attractive method to control osseointegration. Nanotopographical features on a substrate are several orders of magnitude smaller than most mammalian cells, including osteoblasts. They are rather more akin to the scale of cell receptors, such as integrins.[8] Increased cell adhesion, adhesion-related signaling, and cytoskeletal tension have been shown to be important in osteogenesis.[9–11]

Previously, it has been shown that nanoscale disorder in patterning of the cell adhesion integrin ligand, Arginyl-glycyl-aspartic acid (RGD) motif, can be employed to increase cell adhesion.[12] In addition, controlled disorder has been seen to be important in mesenchymal stem cell (MSC) differentiation to osteoblasts.[9,13] Further, features with a height of around 15–20 nm have been seen to provide increased osteogenic effect.[14–16]

Block copolymer self-assembly provides a technique that can produce arrays of slightly disordered, but not random patterns, over large areas in a cost effective and accessible manner. Maclaine et al. showed that using the block copolymer technique to produce control-disorder nanotopographies on thermoplastics was highly osteogenic and cost effective.[17] Furthermore, the technique can be used to make templates through which Ti can be anodized selectively in a polymer domain, e.g., the P4VP in PS-b-P4VP block copolymer, to allow formation of the titanium oxide or titania patterns. The block copolymer patterning allows rapid and inexpensive fabrication over large areas and 3D complex shapes, which may facilitate the use of nanotopography on orthopedic implants in a simpler manner than that, e.g., with electron beam lithography which tends to be a 2D fabrication technique.[16]

In considering integration of bony implants, not only is lack of appropriate bone formation a concern, but osteolysis due to osteoclast activity also contributes to loosening. It is thus critical to understand if bioactive effects of nanotopography are specifically osteogenic or if they are generally activating and thus increase osteoclast activity in hand with increase osteoblast activity. Osteoclasts are derived from the hematopoietic lineage through fusion of macrophage cells. Osteoblast activity stimulates osteoclastogenesis through production of receptor activator of nuclear factor kappa-B ligand (RANKL) and macrophage colony-stimulating factor (M-CSF); thus co-stimulation is potentially an issue.[18–21]

We have previously developed a simple co-culture system comprising human bone marrow stromal cells (BMSCs) and human bone marrow hematopoietic cells (BMHCs).[22] This culture methodology was developed from work on osteoblast cell lines/primary osteoblasts/MSCs with peripheral blood mononuclear cell cultures/isolated monocytes stimulated by M-CSF and RANKL,[23–25] and porcine and human BMSCs and CD34+ hematopoietic progenitors.[21,26–28] This co-culture derived from human bone marrow stromal cells (BMSCs) and human bone marrow hematopoietic cells (BMHCs) allows a better representation in vitro of osteoinductive/osteolytic potential of materials surfaces and thus, in this study, we combine our co-culture with 15 nm high disordered nanofeatures on titanium (Ti) to study potential for implant development. This is also validated in vivo.

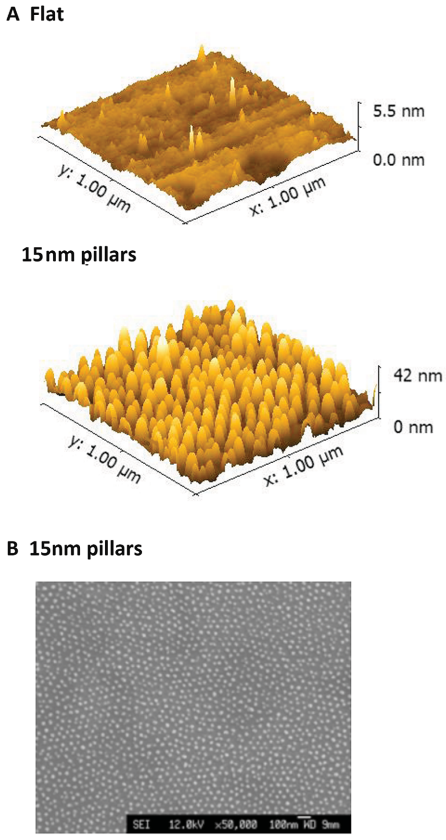

Figure 1. A) 3D AFM height images of Ti surfaces that were anodized at 6 V using the (41.5-b-17.5) × 10^3 g mol^{-1} BCP template. The z-scales have been adjusted to the same scale to visualize the height difference. B) SEM image of the 15 nm TiO_2 pillar substrate. Scale bars as shown.

2. Results and Discussion

2.1. Co-Cultures on Ti Substrates

Previous studies have shown that nanotopographically treated surfaces comprised nanopatterns with controlled disorder (but not randomness) influence MSC differentiation[9,29] using simple in vitro models. Further, Young et al. developed an osteoblast/osteoclast progenitor co-culture where mature phenotypes of both progenitors lines could be observed.[22] Such a co-culture, derived from human bone marrow stromal cells (BMSCs) and human bone marrow hematopoietic cells (BMHCs), and was cultured on 14 mm diameter flat and nanopillar TiO_2 discs. The nanopillars, of 15 nm height, 21 nm diameter, and positioned at 30 nm intervals, shown in **Figure 1**A,B (AFM and SEM, respectively), were fabricated using our block copolymer templated anodization technique. Both detailed chemical analyses and AFM characterization of these surfaces have been published previously.[15,16]

In agreement with our previous work,[16] the cells on all substrates adopted a well spread polygonal morphology and organized architecture (**Figure 2**A). A slightly higher number of cells were counted on the 15 nm pillar surface (Figure 2B)

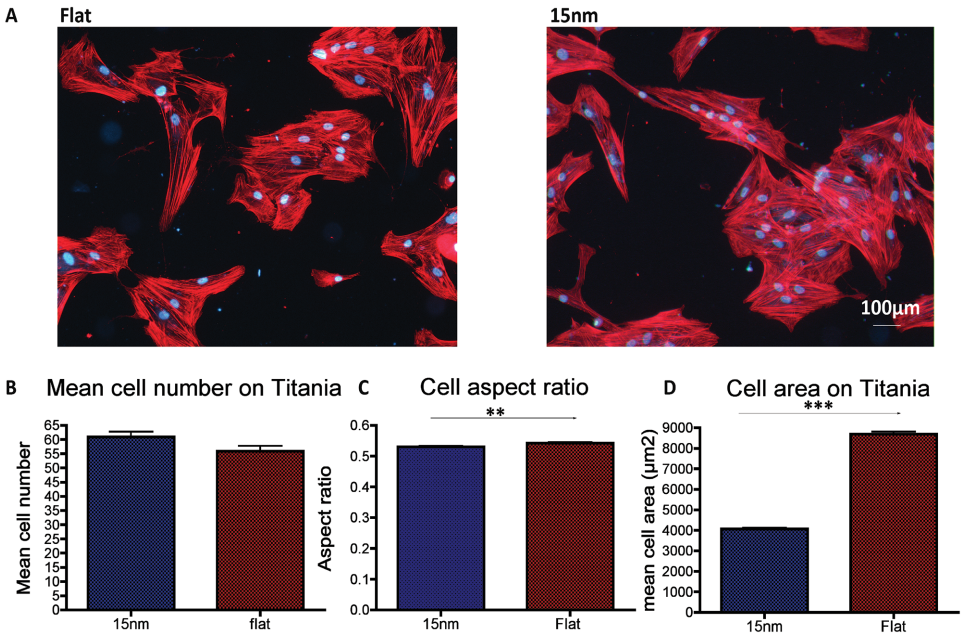

Figure 2. Cell growth on titania. A) Immunofluorescent images of cells on the 15 nm pillars and flat control titania surfaces. Scale 100 µm. B) Similar cell numbers observed on 15 nm pillars and flat control. C) Cell aspect ratio indicated a more elongated cell shape on the 15 nm pillar surface. D) Cell area was highly reduced on the 15 nm pillar in comparison to the control cultures. $n = 30$ frames. Results shown ±SEM. Comparison was done by unpaired *t*-test, $^{**}p < 0.01$, $^{***}p < 0.001$.

and they appeared polarized and elongated, as they displayed a smaller aspect ratio (calculated as ratio of cell minor axis versus major axis), in comparison to the cells growing on the control surface (Figure 2C, $p < 0.05$). Measurements of cell area indicated a statistically significant reduction in cell spreading on the 15 nm pillars (Figure 2D, $p < 0.05$). Furthermore, we have shown that cells grown on the 15 nm pillars form larger focal adhesions than the control surface.[16] These results are features of typical osteogenic cells and agree with our previous data on osteoinductive, slightly disordered nanodots NSQ50.[11,29]

In order to evaluate the effects of the 15 nm pillars on osteoblastogenesis and osteoclastogenesis, several genes were assessed by quantitative reverse transcription polymerase chain reaction (qRT-PCR) (**Figure 3**). A statistically significant ($p < 0.05$) increase in the expression of the alkaline phosphatase (ALP) osteoblast marker transcript was observed in the co-cultures on the 15 nm pillars as compared to the flat control over time (Figure 3B).

The expression of osteoprotegerin (OPG), a negative regulator of osteoclastogenesis osteoclast differentiation, was found statistically significantly ($p < 0.05$) upregulated in co-cultures on the 15 nm pillars in a time related manner (Figure 3C). OPG protects the bones from excessive bone resorption by selective binding to the RANK ligand, RANKL, preventing it from binding to its receptor.[20] This, RANKL/OPG ratio is crucial for bone turnover.[19] Interestingly, as OPG expression was increased from day 14 to day 28 on the 15 nm TiO_2 pillars (Figure 3C), RANKL expression was reduced (Figure 3I). Concomitantly, the expression of the osteoclast marker tartrate resistant acid phosphatase (TRAP) was found significantly ($p < 0.05$) decreased in cells on the 15 nm pillars when compared to cells on the control (Figure 3H). Analysis of the expression of other osteoclast specific genes osteoclast-associated receptor (OSCAR), Cathepsin K and tumor suppressor gene α (TNFα) showed a trend of reduced expression with time on the nanopillar surface but no statistical difference to the control surface, again suggestive of a reduced osteoclastogenesis in response to the nanopillars. Expression of the cytokine IL-6 was found to be statistically significantly ($p < 0.05$) increased in the 15 nm pillars when compared to the control (Figure 3D) in the co-cultures. IL-6 is involved in bone remodeling and can have positive effects on both osteoblastogenesis and osteoclastogenesis.[30,31]

In order to assess if the genomic differences observed are translated at the protein level a combination of histo- and immunostaining was performed. In a first instance, Alizarin red staining was performed to allow quantitative assessment of calcium deposition in bone nodule deposition (**Figure 4**). At day 28, both nanopillar and flat Ti substrates showed widespread calcium deposition when analyzed by the Alizarin red stain (Figure 4A). Statistical analysis was performed by unpaired *t*-test with Welch's correction. A significant difference was observed between the two substrates ($p < 0.05$), demonstrating greater nodule formation from cells on 15 nm features compared to cells on flat control.

Immunofluorescence staining for osteopontin (OPN), an osteoblast marker was performed on the co-cultures at day 28. Figure 4B shows a graphical illustration of osteopontin mean intensity on both substrates. A statistically significant increase in OPN expression was noted for cells on the nanopillar substrate, in comparison to those on the flat control.

Histochemical TRAP staining was performed in order to look for topographically induced changes in osteoclastogenesis. In agreement with the gene expression results, significantly

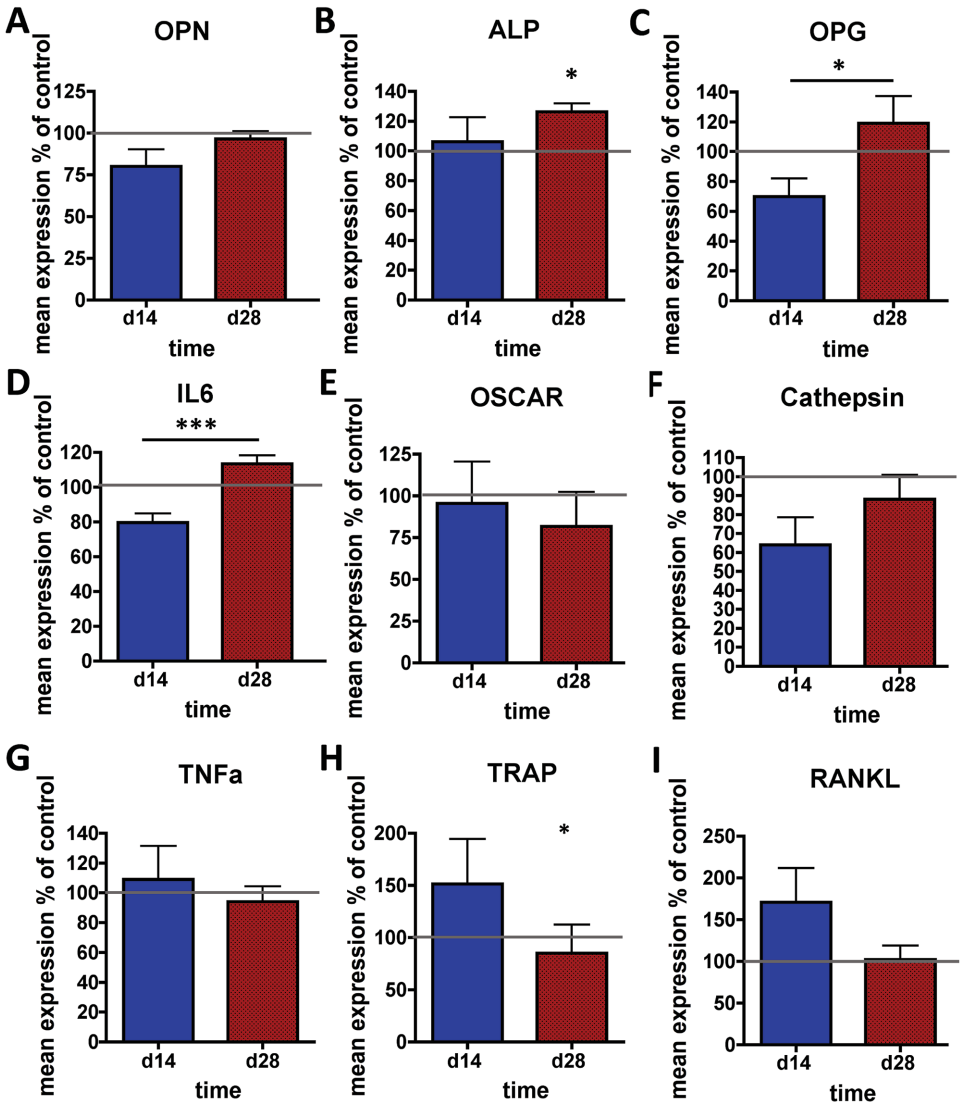

Figure 3. Mean gene expression in co-cultures on the 15 nm nanopillar TiO_2 substrate in comparison to on the flat Ti control at day 14 and 28 time points. A) Osteopontin (OPN), B) alkaline phosphatase (ALP), C) osteoprotegrin (OPG), D) interleukin-6 (IL-6), E) OSCAR, F) Cathepsin-K, G) tumor necrosis factor alpha (TNFα), H) tartrate resistant acid phosphatase (TRAP), and I) RANKL. Results are shown as percentage of the relevant flat control (set at 100) for each time point. $n = 3$ patients and results shown ±SEM. Comparison was done by ANOVA $^*p < 0.05$, $^{***}p < 0.001$.

decreased ($p < 0.05$) levels of TRAP positive cells were noted in the co-culture on the 15 nm pillars substrate in comparison to the flat control (**Figure 5**A,B). Figure 5C shows mature osteoclasts with the typical large circular morphology and multiple nuclei.

SEM imaging confirmed the gene and protein results. On the planar control, a viable co-culture of well spread BMSCs and rounded BMHCs at days 14 and 28 can be seen (**Figure 6**A,C). However, for cultures on the 15 nm pillars, very few BMHCs were noted (Figure 6B) and where they were, they tended to be adhered to spread BMSCs rather than the substrate (Figure 6D).

2.2. In Vivo Bone to Implant Contact (BIC) Assessment

In order to assess the osteointegration potential of the nanopattern, 15 nm pillar titanium implants and appropriate planar controls were implanted into rabbit femora. It was seen that the bone to implant contact (BIC) rate was ≈20% higher in the nanopillar surfaces as compared to the flat control demonstrating an osteointegrative effect of the nanopillar surface (**Figure 7**).

3. Summary

Previous studies have shown that nanotopographically treated surfaces comprised nanopatterns with controlled disorder (but not randomness) influence MSC differentiation using simple in vitro models.[9,11,29] Further, Young et al. developed an osteoblast/osteoclast progenitor co-culture where mature phenotypes of both progenitors lines could be observed[22] and we have adopted that culture system for this new report on controlled titanium nanopatterns. Our data show that 15 nm high

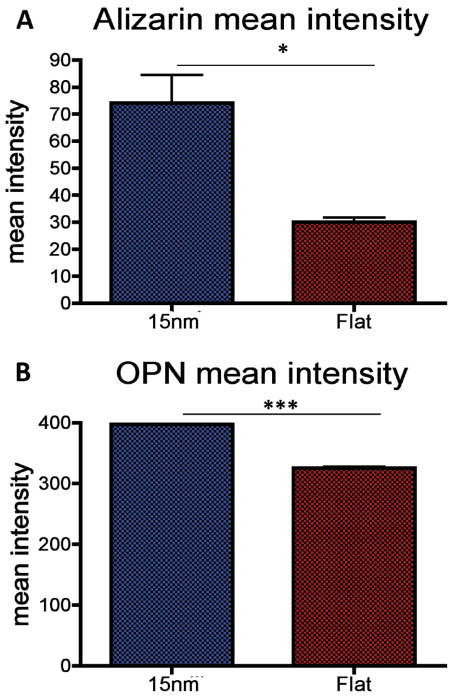

Figure 4. Immunostaining for osteogenesis. A) Alizarin red staining mean intensity demonstrating statistically significant increased osteoblast activity on the nanopillar substrate in comparison to the flat control ($n = 5$). B) Osteopontin (OPN) mean intensity increased in the 15 nm pillars in comparison to the flat control ($n = 30$). Results shown ±SEM. Comparison was done by unpaired t-test, $*p < 0.05$, $***p < 0.001$.

disordered nanopillars increase osteogenesis (as shown by ALP, osteopontin, and mineralization studies) without increasing osteoclastogenesis (as shown by qRT-PCR for osteoclast related genes and TRAP staining); i.e., it is specifically bioactive to bone formation rather than generally bioactive to all cell types in contact. This is clearly important as increased bone contact without increased resorption would be an implant ideal.

It is important to consider building complexity into in vitro bone/implant analysis as osteointegration is a complex process involving interplay of osteolytic and osteogenic processes. While individual pathways for osteolysis and osteoinduction have been described, the process of bone remodeling has many different signaling pathways which are dynamic, depending on the presence of other cells, pathways or nanotopographical features in the immediate environment.

As well as moving to understand more the interplay of these cells and if our nanotopography is specifically or generally bioactive, we produce in vivo data to verify these in vitro findings. Again, the osteogenic properties of the nanopillar substrate were clearly demonstrated, with a significant increase in the bone to implant contact in comparison to polished titanium, again demonstrating the potential of the nanopatterns.

Previously in vivo findings related to nanoscale topography have focused on nanoscale/sub-μm roughness rather than controlled nanotopography and have shown positive effects on bone formation are achievable.[32–35] Our block copolymer template anodization technique, however, provides reproducible nanotopography that should allow for consistency of effect which is important when focusing on translation to implants for human

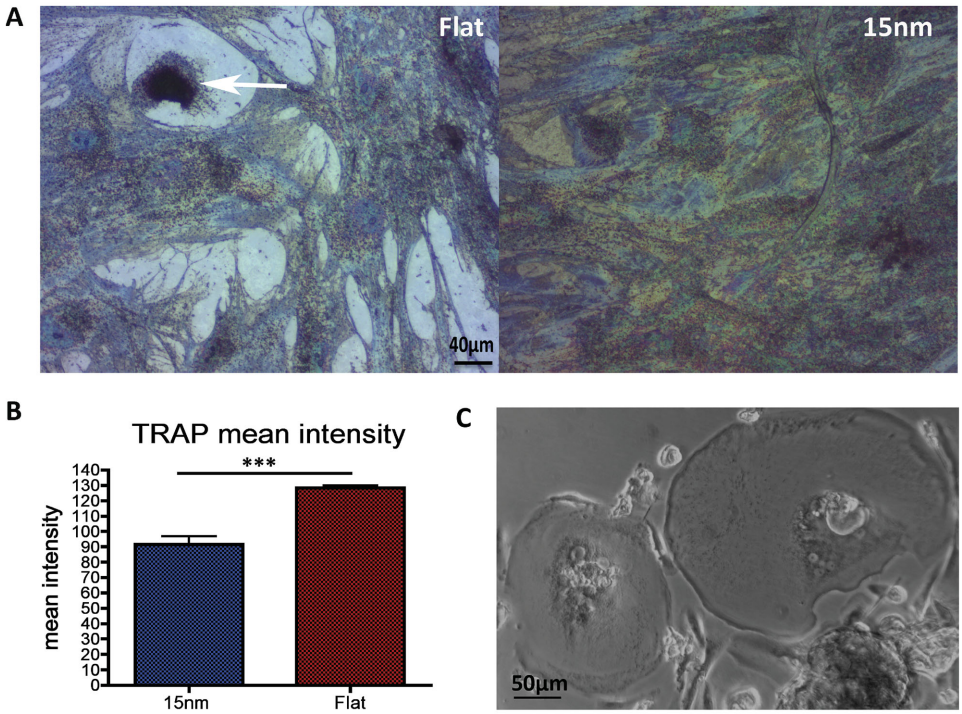

Figure 5. TRAP histochemical images. A) Flat and nanopillar substrate respectively, 20× magnification. Images show TRAP positive macrophages or preosteoclasts indicative of osteoclastic activity on the flat substrate. No TRAP positive macrophages were seen on the nanopillar substrate. B) TRAP staining mean intensity was statistically significantly lower in the 15 nm pillars versus the flat control as measured by an unpaired t-test, $***p < 0.001$. $n = 8$ and results shown ±SEM. C) Representative image of mature osteoclasts.

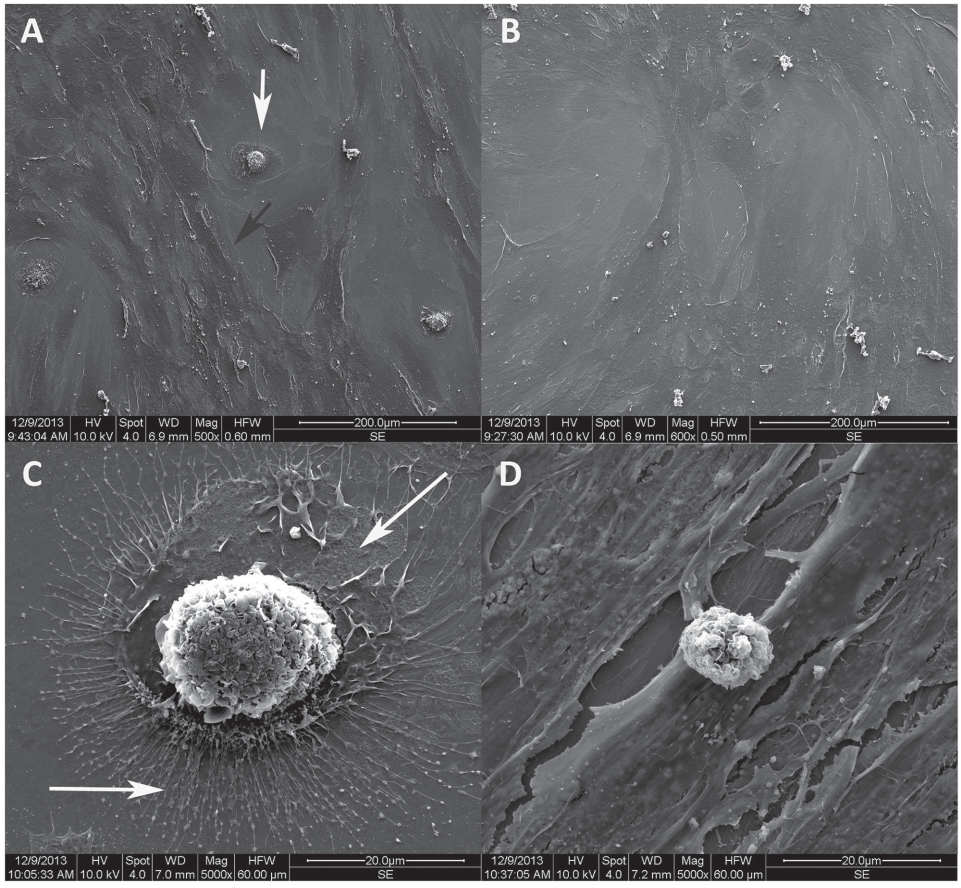

Figure 6. SEM of A) flat Ti substrate at day 28, 500× magnification osteoclast progenitors (white arrow), osteoblasts (dark arrow) are shown. B) Nanopillar Ti substrate at day 28, 600× magnification. C) Flat Ti substrate at day 28, 5000 x magnification. D) Nanopillar substrate at day 28, 5000× magnification. Images (A) and (B) demonstrate the evidence of co-culture of osteoblasts and osteoclast progenitors, with a decrease in osteoclast progenitor cells on the 15 nm pillars versus the flat substrate. Image (C) shows an osteoclast progenitor cell on the flat substrate with lamellipodia (upper arrow), filopodia (lower arrow), and phagocytic pits. A less mature osteoclast progenitor cell is seen in image (D), and is seen to be adherent to osteoblast cell, not the nanopillar substrate surface.

use; two similar Ra values can belong to very different looking topographies and so roughness alone can be an unsatisfactory descriptor. This allowed us to study minute changes of nanodot dimensions, namely 8 nm height versus 15 nm height, on cell behavior.[16] Further, the anodization technique only results in minimal changes in surface chemistry,[15] allowing the study of the influence of nanotopography on its own.

Assessment under in vitro co-culture and in vivo animal models has demonstrated the osteogenic properties of 15 nm nanopillar on Ti substrate without an associated osteoclastic response. This is encouraging for developing orthopedic implants which have improved osteointegration, survivorship, and reduced revision surgery rates. The successful co-culture on Ti provides improved in vitro analysis of the implant–bone environment and is a potential standard for laboratory assessment of new substrates.

4. Conclusion

A viable co-culture was developed on titanium flat and 15 nm high nanopillar substrates. Qualitative and quantitative analyses demonstrated improved bone deposition without unwanted osteoclastogenesis on the 15 nm nanopillars. This, together with increased in vivo osseointegration, demonstrates good potential for orthopedic implant applications.

5. Experimental Section

Substrate Fabrication: Nanopatterning of the Ti surfaces was performed according to previous work.[15] 14 mm diameter Ti disks (ASTM grade 1, Titanium Metals UK Ltd.) were mirror polished. Poly(styrene-b-4-vinylpyridine) (PS-b-P4VP) with molecular weight 41.5-b-17.5 $\times$ 10^3 g mol^{-1} (Polymer Source) was dissolved in a mixture of toluene and tetrahydrofuran (THF) (70/30) to a concentration of 0.5 wt%. A thin film of the polymer solution was formed on the Ti disks by spin-coating at 2000 rpm and subsequently solvent annealed in THF vapor for 3 h. The Ti samples were then anodized at 10 V in 0.01 M oxalic acid and finally the polymer template was removed using an O_2 plasma. The resulting nanopillars had a height of 15 nm and an average distance of 30 nm. Mirror polished Ti disks were used as control surfaces.

Human Bone Marrow Stromal Cells (BMSCs) and Human Bone Marrow Hematopoietic *Cells (BMHCs) Isolation*: Bone marrow (BM) was harvested from healthy patients undergoing hip and knee arthroplasty (informed signed consent has been obtained from the participants)

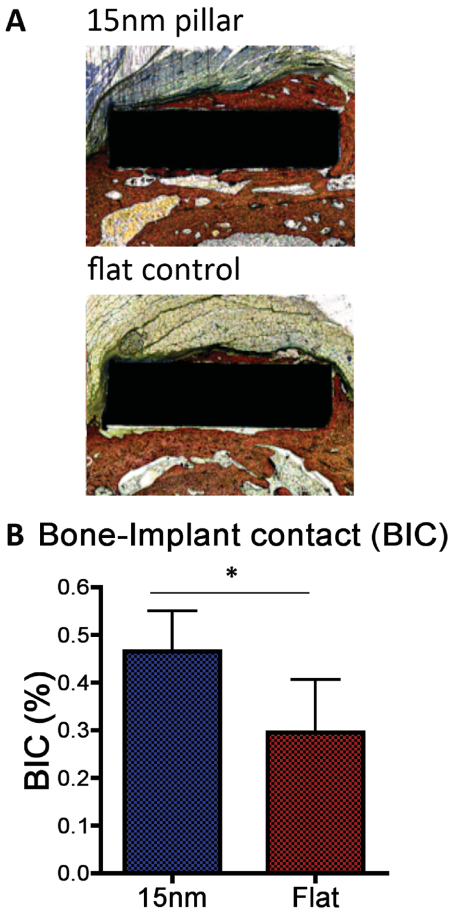

Figure 7. Histological staining results of rabbit femur/implant interface. A) Images of staining with Stevenel's Blue, and counter staining with Van Gieson stain indicated increased bone–implant contact as shown by the increased bone growth around the implant. These specimens were evaluated by optical microscope (Olympus BX41, Olympus Co., Japan) and image analysis software (Osteomeasure Software, Osteometric Inc., USA) to allow a quantitative measurement of the bone to implant contact (BIC). B) Graphical representation of BIC between groups. $n = 5$ and results shown ±SEM unpaired t-test, $*p < 0.05$.

and stored in (phosphate buffered saline (PBS), 0.53×10^{-3} M EDTA and antibiotics (6.74 U mL^{-1} Penicillin-Streptomycin, 0.2 µg mL^{-1} Fungizone)). BM aspirate was washed and cultured in basal media (DMEM (Sigma), 10% fetal bovine serum, 100×10^{-3} M sodium pyruvate, 200×10^{-3} M L-glutamine (Invitrogen), 1% MEM NEAA (Gibco), and antibiotics. The aspirate was then centrifuged at 376× g for 10 min. This sequence was repeated twice. The cell pellets were resuspended in medium and overlaid on a Ficoll gradient. This was then centrifuged at 445 g for 45 min. The mononuclear interface layer aspirated and resuspended in medium. The cells were further washed and transferred in an appropriate sized cell culture flask and incubated at 37 °C with 5% humidified CO_2. At day 3, the nonadherent cells were removed and cultured separately as HSCs. The remaining adherent cells were cultured further for 7–10 d until a confluent BMSC layer was identified. This was repeated three times using BM from three different patients to ensure reproducibility.

Co-Cultures on Titania Nanopillar Surfaces: Following 7–10 d of culture, the adherent BMSCs were detached by washing twice with HEPES saline followed by a 4 min incubation at 37 °C in a trypsin solution (0.05% trypsin/0.53×10^{-3} M EDTA). The enzyme was stopped by the addition of fresh culture medium, the cells were then centrifuged, counted, and resuspended in mDMEM to a concentration of 1×10^4 cells per mL. 1 mL of the cell suspension was pipetted directly onto the prepared TiO_2 substrates. After 7 d of culture, 1 mL of BMHCs suspension was added at a concentration of 1.5×10^5 cells per mL. This created the co-culture.

Scanning Electron Microscopy (SEM): SEM was performed at days 14 and 28 of co-culture on two 15 nm nanopillar TiO_2 and two polished Ti substrates for each time point. Cells were fixed in 4% glutaraldehyde, followed by a wash stage in 0.2 M sodium cacodylate (pH 7.4). The substrates were then post fixed in 1% osmium tetroxide in sodium cacodylate buffer, and then washed again in sodium cacodylate buffer. The substrates were then immersed in a 1% tannic acid in 0.1 M sodium cacodylate solution for 60 min. This was followed by a further wash in 0.2 M sodium cacodylate. Dehydration through an incremental alcohol series followed by hexamethyldisiloxane was conducted prior to sputter coating (20 nm gold/palladium) and viewing with Zeiss Sigma FE-SEM microscope.

Atomic Force Microscopy (AFM): The surfaces were characterized using AFM (Veeco Multimode with Quadrex Nanoscope 3D system) and FEG-SEM (JEOL JSM 6330F). The nanodots height was retrieved from AFM cross-sectional profiles.

Histochemistry: A—TRAP Staining. At day 28 of co-culture, histochemical analysis was performed on two nanopillar and two flat substrates. Cells were fixed with 4% formaldehyde for 30 s and then stained for TRAP, (Acid Phosphatase Leukocyte No.387, Sigma-Aldrich). Samples were also counterstained for 10 min in hematoxylin solution and washed with H_2O. TRAP staining allows assessment of osteoclastogenesis, as TRAP is expressed by osteoclast cells and their progenitors.

Histochemistry: B— Alizarin Staining: Alizarin red stain (pH 4) of 2% (w/v) was prepared (Alizarin red S (Sigma)) in dH_2O. Cells were fixed in 4% formaldehyde for 15 min and then stained for 5 min before H_2O and PBS rinses. Samples were assessed by bright-field optical microscopy. Alizarin red staining assesses calcium deposition and thus osteoblastogenesis.

For both TRAP and Alizarin red stains, comparisons of staining intensity between substrates were analyzed by Image J software.

Immunofluorescence: At day 28, two discs of each substrate were analyzed by immunofluorescence staining. Cells were fixed (4% formaldehyde/phosphate-buffered saline (PBS) with 1% sucrose) at 37 °C for 15 min. The fixative was then removed and the samples were permeabilized (10.3 g of sucrose, 0.292 g of NaCl, 0.06 g of $MgCl_2$, 0.476 g of HEPES buffer, 0.5 mL of Triton X, in 100 mL of 1 x PBS, pH 7.2) at 4 °C for 5 min. This was followed by a blocking step with 1% bovine serum albumin (BSA)/PBS at 37 °C, for 5 min. Anti-osteopontin (1:100 in 1% BSA/PBS, AKm2A1 (osteopontin, Autogen Bioclear, UK) mouse monoclonal antihuman antibody (IgG1)) was added for 1 h (37 °C). The samples were co-stained with fluorescein isothiocyanate (FITC)-conjugated phalloidin (1:100 Invitrogen, UK). The samples were then washed in 1 x PBS/0.5% Tween 20 (3 × 5 min at room temperature). A secondary, biotin-conjugated antibody (1:50 in 1% BSA/PBS, monoclonal horse antimouse (IgG), Vector Laboratories, Peterborough, UK) was added for 1 h (37 °C) followed by washing. A third, Cy-3 conjugated streptavidin, layer was added (1:50, Vector Laboratories, Peterborough, UK) at 4 °C for 30 min, before the samples were given a final wash and mounted in Vectashield mounting medium (Vector labs) containing 4',6-diamidino-2-phenylindole (DAPI) to stain the nucleus. Visualization was via a fluorescence microscope (Zeiss Axiovert 200 M, 10× magnification, NA 0.5). Image J was used for the data acquisition of OPN staining intensity from the different substrates. The CellProfiler software suite (Broad Institute, USA) was used to process over 30 image sets, acquired using an inverted fluorescence microscope (Olympus). An image processing pipeline was generated to load the DNA (DAPI), actin (phalloidin-rhodamine), and antibody stain (fluorescein), followed by automated detection of cell morphology, area, and cell aspect ratio.

qRT-PCR: Total RNA from both day 14 and 28 time points cultures was extracted using a Qiagen RNeasy micro kit according to the manufacturer's protocol. Equal amount of RNA from each sample was used for cDNA preparation using the QuantiTect RT-PCR kit from

Table 1. PCR primer sequences.

Target gene	Forward sequence	Reverse sequence
OSCAR	CCAGCTCTAGCGGGTATCTG	GACGGAGTGATGTCTGTGTGAC
Osteoprotegrin	GAAGGGCGCTACCTTGAGAT	GCAAACTGTATTTCGCTCTGG
RANKL	TGATTCATGTAGGAGAATTA-AACAGG	GATGTGCTGTGATCCAACGA
IL-6	GATGAGTACAAAAGTCCT-GATCCA	CTGCAGCCACTGGTTCTGT
TRAP	GGACTGAAGGGACTCCTGAAT	GGTCCCTGAGCCTTTATTCC
TNFα	CAGCCTCTTCTCCTTCCTGAT	GCCAGAGGGCTGATTAGAGA
Cathepsin-K	GCCAGACAACAGATTTCCATC	CAGAGCAAAGCTCACCACAG
Alkaline Phosphatase	AGAACCCCAAAGGCTTCTTC	CTTGGCTTTTCCTTCATGGT
Osteopontin	AGCTGGATGACCAGAGTGCT	TGAAATTCATGGCTGTGGAA
GapDH	GTCAGTGGTGGACCT-GACCT	ACCTGGTGCTCAGTGTAGCC

Qiagen following the Qiagen protocol. qRT-PCR was carried out using the Quantifast SYBR Green kit (Qiagen)and the 7500 Real Time PCR system from Applied Biosystems. The GapDH housekeeping gene primer set was used for normalization. Three to four replicates were tested at each time point with the calculated mean normalized against GapDH. OSCAR, Osteoprotegrin, RANKL, IL-6, TRAP, TNF-α, Cathepsin-K, OPN, and Alkaline phosphatase primers were used for analysis. The primer sequences (**Table 1**) for the genes were validated by dissociation curve/melt curve analysis.

Implantation of Surface-Treated Metal Materials in Rabbits: In vivo studies were performed with the approval of the Animal Experimentation Ethics Committee of The Chinese University of Hong Kong. Five New Zealand male 8-week-old white rabbits underwent the surgery. Under the general anesthesia, two materials with different coating were randomly implanted on the anterior side of right femur of the animals. All the animals were terminated and femora with materials were harvested two months after the implantation surgery. All the samples were embedded into methylmethacrylate (MMA) before sliced. BIC was quantitatively measured by Osteomeasure software.

Material Implant Surgery: All the animals were anesthetized with a mixture of ketamine (35 mg kg^{-1}) and xylazine (5 mg kg^{-1}) intramuscularly. Femora were exposed via longitudinal skin incision on the lateral side of hind limb. Three grooves (0.8 × 0.8 cm in area; 0.1 cm in depth; 1 cm in interval) were created by an abrasive drill to make the bone surface rough. Two different kinds of materials were implanted in the grooves randomly and covered with periosteum separately. Finally, wounds were closed in layers. All rabbits were injected with penicillin (800 000 units) intramuscularly once per day for 3 d after surgery.

Histological Evaluation of Rabbit Tissues: Femora were harvested and fixed in 4% paraformaldehyde (pH 7.4) for 48 h after sacrifice. Then, all the samples were placed in 70% ethanol for further dehydration in graded ethanol and embedded in MMA to produce undercalcified bone sections. The infiltration process was carried out by placing the bone specimens into a solution of MMA and dibutylphtalate (3:1) for 48 h, followed by another 48 h in MMA. Embedding of the infiltrated specimens was done in fresh MMA, dibutylphtalate (3:1) and 2.5% benzoyl peroxide solution at 20 °C. Polymerization was completed within 48 h. Attempts were made to standardize the sectioning at a mid-sagittal plane of each specimen by cutting the specimen in half (transversely in a coronal plane) using a low-speed diamond saw (Leica SP1600, Leica Company, Germany), and the MMA sections were then polished to thin MMA sections (100 μm). For histological examination, MMA slices were stained with Stevenel's Blue, and counter stained with Van Gieson stain. These specimens were evaluated by optical microscope (Olympus BX41, Olympus Co., Japan) and image analysis software (Osteomeasure Software, Osteometric Inc., USA) to allow a quantitative measurement of the BIC.

Statistical Analysis: After analysis by Image J software, statistical analysis of Alizarin Red and TRAP histochemical staining was performed by the student's *t*-test. The student's *t*-test was again utilized for analysis of the immunofluorescence results.

Statistical analysis of qPCR was performed by the two-way ANOVA (analysis of multiple variance) test.

Statistical analyses of in vivo rabbit experiments were performed by student's *t*-test. All data are presented as $\overline{X} \pm S$. The level of statistical significance was set at $p < 0.05$.

DOI for data citation: http://dx.doi.org/10.5525/gla.researchdata.211

Acknowledgements

This work was supported by EPSRC grant EP/K034898/1 and EP/K035142/1. The authors thank financial support from the National Natural Science Foundation of China (81371946) and Hong Kong Government Research Grant Council, General Research Fund (Grant No. CUHK470813) to Gang Li for the research work. This study was also supported, in part, by SMART program, Lui Che Woo Institute of Innovative Medicine, Faculty of Medicine, and The Chinese University of Hong Kong. We would like to thank Mrs Carol-Anne Smith for technical laboratory assistance, Mrs. Margaret Mullin and Dr. Peter Chung for the SEM work. The authors declare no conflict of interest. The authors have no other relevant affiliations or financial involvement with any organization or entity with a financial interest in or financial conflict with the subject matter or materials discussed in the manuscript apart from those disclosed. No writing assistance was utilized in the production of this manuscript.

Received: August 20, 2015
Revised: October 5, 2015
Published online: February 18, 2016

[1] P. E. Purdue, P. Koulouvaris, B. J. Nestor, T. P. Sculco, *HSS J.* **2006**, *2*, 102.
[2] R. Glass, M. Arnold, E. A. Cavalcanti-Adam, J. Blümmel, C. Haferkemper, C. Dodd, J. P. Spatz, *New J. Phys.* **2004**, *6*, 101.
[3] D. S. W. Benoit, M. P. Schwartz, A. R. Durney, K. S. Anseth, *Nat. Mater.* **2008**, *7*, 816.
[4] J. M. Curran, R. Stokes, E. Irvine, D. Graham, N. A. Amro, R. G. Sanedrin, H. Jamil, J. A. Hunt, *Lab Chip* **2010**, *10*, 1662.
[5] A. J. Engler, S. Sen, H. L. Sweeney, D. E. Discher, *Cell* **2006**, *126*, 677.
[6] R. McBeath, D. M. Pirone, C. M. Nelson, K. Bhadriraju, C. S. Chen, *Dev. Cell* **2004**, *6*, 483.
[7] R. J. McMurray, N. Gadegaard, P. M. Tsimbouri, K. V. Burgess, L. E. McNamara, R. Tare, K. Murawski, E. Kingham, R. O. Oreffo, M. J. Dalby, *Nat. Mater.* **2011**, *10*, 637.
[8] M. J. Dalby, N. Gadegaard, R. O. Oreffo, *Nat. Mater.* **2014**, *13*, 558.
[9] M. J. Dalby, N. Gadegaard, R. Tare, A. Andar, M. O. Riehle, P. Herzyk, C. D. W. Wilkinson, R. O. C. Oreffo, *Nat. Mater.* **2007**, *6*, 997.
[10] K. A. Kilian, B. Bugarija, B. T. Lahn, M. Mrksich, *Proc. Natl. Acad. Sci. USA* **2010**, *107*, 4872.
[11] P. M. Tsimbouri, R. J. McMurray, K. V. Burgess, E. V. Alakpa, P. M. Reynolds, K. Murawski, E. Kingham, R. O. Oreffo, N. Gadegaard, M. J. Dalby, *ACS Nano* **2012**, *6*, 10239.
[12] J. Huang, S. V. Grater, F. Corbellini, S. Rinck, E. Bock, R. Kemkemer, H. Kessler, J. Ding, J. P. Spatz, *Nano Lett.* **2009**, *9*, 1111.

[13] P. M. Tsimbouri, K. Murawski, G. Hamilton, P. Herzyk, R. O. Oreffo, N. Gadegaard, M. J. Dalby, *Biomaterials* **2013**, *34*, 2177.
[14] L. E. McNamara, T. Sjöström, K. E. Burgess, J. J. Kim, E. Liu, S. Gordonov, P. V. Moghe, R. D. Meek, R. O. Oreffo, B. Su, et al., *Biomaterials* **2011**, *32*, 7403.
[15] T. Sjöström, L. E. McNamara, L. Yang, M. J. Dalby, B. Su, *ACS Appl. Mater. Interfaces* **2012**, *4*, 6354.
[16] T. Sjöström, L. E. McNamara, R. M. D. Meek, M. J. Dalby, B. Su, *Adv. Healthc. Mater.* **2013**, *2*, 1285.
[17] S. E. Maclaine, N. Gadhari, R. Pugin, R. M. D. Meek, M. Liley, M. J. Dalby, *J. Orthop. Res.* **2012**, *30*, 1190.
[18] S. E. Haynesworth, M. A. Baber, A. I. Caplan, *J. Cell. Physiol.* **1996**, *166*, 585.
[19] K. Matsuo, N. Irie, *Arch. Biochem. Biophys.* **2008**, *473*, 201.
[20] G. R. Mundy, B. Boyce, D. Hughes, K. Wright, L. Bonewald, S. Dallas, S. Harris, N. Ghosh-Choudhury, D. Chen, C. Dunstan, *Bone* **1995**, *17*, 71S.
[21] K. Nakagawa, H. Abukawa, M. Y. Shin, H. Terai, M. J. Troulis, J. P. Vacanti, *Tissue Eng.* **2004**, *10*, 93.
[22] P. Young, P. Tsimbouri, N. Gadegaard, R. Meek, M. Dalby, *Nanomedicine* **2015**, *10*, 949.
[23] V. Bloemen, T. J. de Vries, T. Schoenmaker, V. Everts, *Biochem. Biophys. Res. Commun.* **2009**, *385*, 640.
[24] S. Greiner, A. Kadow-Romacker, G. Schmidmaier, B. Wildemann, *J. Biomed. Mater. Res. A* **2009**, *91*, 288.
[25] G. L. Jones, A. Motta, M. J. Marshall, A. J. El Haj, S. H. Cartmell, *Biomaterials* **2009**, *30*, 5376.
[26] A. Bernhardt, S. Thieme, H. Domaschke, A. Springer, A. Rösen-Wolff, M. Gelinsky, *J. Biomed. Mater. Res. A* **2010**, *95*, 848.
[27] C. Heinemann, S. Heinemann, H. Worch, T. Hanke, *Eur. Cell. Mater.* **2011**, *21*, 80.
[28] G. Mbalaviele, N. Jaiswal, A. Meng, L. Cheng, C. Van Den Bos, M. Thiede, *Endocrinology* **1999**, *140*, 3736.
[29] P. Tsimbouri, N. Gadegaard, K. Burgess, K. White, P. Reynolds, P. Herzyk, R. Oreffo, M. J. Dalby, *J. Cell. Biochem.* **2014**, *115*, 380.
[30] F. Blanchard, L. Duplomb, M. Baud'huin, B. Brounais, *Cytokine Growth Factor Rev.* **2009**, *20*, 19.
[31] F. Yoshitake, S. Itoh, H. Narita, K. Ishihara, S. Ebisu, *J. Biol. Chem.* **2008**, *283*, 11535.
[32] S. Lavenus, V. Trichet, S. Le Chevalier, A. Hoornaert, G. Louarn, P. Layrolle, *Nanomedicine* **2012**, *7*, 967.
[33] E. Rieger, A. Dupret-Bories, L. Salou, M.-H. Metz-Boutigue, P. Layrolle, C. Debry, P. Lavalle, N. Engin Vrana, *Nanoscale* **2015**, *7*, 9908.
[34] L. Salou, A. Hoornaert, J. Stanovici, S. Briand, G. Louarn, P. Layrolle, *Nanomedicine* **2015**, *10*, 741.
[35] L. Salou, A. Hoornaert, G. Louarn, P. Layrolle, *Acta Biomater.* **2015**, *11*, 494.